# Spectroscopic Characterization of Peroxynitrous Acid in cis-perp Configurations

**Eunice X. J. Li, Ian M. Konen, and Marsha I. Lester***

*Department of Chemistry, University of Pennsylvania, Philadelphia, Pennsylvania 19104-6323*

**Anne B. McCoy***

*Department of Chemistry, The Ohio State University, 100 W. 18th Ave., Columbus, Ohio 43210*

*Received: November 30, 2005; In Final Form: March 4, 2006*

This paper presents experimental evidence, supported by two-dimensional theoretical calculations, that HOONO can be observed in cis−perp (cp) configurations in a pulsed supersonic expansion. The spectral properties (transition frequency, rotational constants, and transition type) of OH overtone transitions originating from a state with predominately cp character are predicted theoretically and compared with those associated with a weak feature at 6996.2 $cm^{-1}$ observed experimentally using infrared action spectroscopy. This spectral feature is attributed to HOONO in cp configurations based on its vibrational frequency, rotational band contour, and resultant OH product state distribution.

## Introduction

The three-body association reaction of OH with $NO_2$ is a key radical termination step in the lower atmosphere.[1] The primary product of this reaction is nitric acid ($HONO_2$),

$$OH + NO_2 + M \rightarrow HONO_2 + M$$

a chemically inactive and photochemically stable product. Kinetic studies over a wide range of pressure (for the bath gas M) and temperature conditions have shown that peroxynitrous acid (HOONO), a less stable isomer of $HONO_2$, can also be formed as a secondary product of this reaction.[2−5] Under atmospheric conditions, HOONO is formed reversibly

$$OH + NO_2 + M \rightleftarrows HOONO + M$$

and is estimated to account for up to 20% of the yield near the tropopause.[5]

Ab initio studies have predicted that there are at least two stable conformations of HOONO,[5−8] namely, the trans-perp (tp) conformer with an extended open structure and the cis-cis (cc) conformer with a five-membered ring-like structure, which are depicted in Figure 1. The cc global minimum structure is computed to have an increased stability of 3.4 kcal $mol^{-1}$ compared to tp-HOONO (including zero-point corrections).[8] The cc-conformer has an intramolecular hydrogen bond between the terminal hydrogen and oxygen atoms, which increases its rigidity and stability, and also has the effect of significantly shifting its OH stretching frequency to lower energy.

Spectroscopic identification of HOONO in the gas phase had been elusive until recently, although it had been previously detected in matrices.[9−11] Starting in 2002, several groups have observed the cc- and tp-conformers of HOONO in the gas phase under thermal flow cell[8,12−18] and jet-cooled conditions.[19−21] The observations have been made using infrared action spectroscopy,[12−15,19−21] cavity ring-down absorption,[8,16] and microwave techniques,[17,18] with complementary ab initio calculations carried out in many cases to aid in assignments.

Experiments have shown that the tp-conformer has a stability of 16.2(1) kcal $mol^{-1}$ relative to the OH + $NO_2$ asymptote,[20] the cc-conformer has a stability of 19.8(2) kcal $mol^{-1}$ derived from kinetic studies[4] and 19.9(5) kcal $mol^{-1}$ deduced from spectroscopic measurements,[15] and a substantial barrier (≥13 kcal $mol^{-1}$)[22] in the perp-perp (pp) configuration separates the two conformers (see Figure 1).[13] There has been considerable debate in the literature as to whether there is a third stable conformer of HOONO in the cis-perp (cp) configuration.[6,7,22,23] Nevertheless, there is ample evidence that torsional excitation of cc-HOONO can break the intramolecular hydrogen bond and thereby access cp-like configurations, as seen in thermal spectra.[15,16]

The theoretical identification of the stable conformers of HOONO has a long history, which was recently reviewed.[16] A central question that remains is whether cp-HOONO exists as a stable conformer. In the absence of the hydrogen bonding interaction, which leads to the cc-HOONO conformer being the most stable, one would anticipate that cp-HOONO would correspond to a minimum on the potential. This is seen in the more general ROONO species, for example, R = $CH_3$.[5,24−26] In the potential surfaces for HOONO recently reported by McCoy et al. (at the CCSD(T) level of theory with cc-pVTZ and cc-pVQZ basis sets),[16] Matthews and Sinha (CCSD(T)/cc-pVTZ),[15] and McGrath and Rowland (using BLYP, B3LYP, and CCSD(T) potentials with diffuse functions such as the avtz basis set),[22] cp-HOONO appears to be a minimum on the potential, but the barrier between this minimum and the global cc-HOONO minimum is very small or zero. More recent calculations by Varner and Stanton (using the CCSD(T) level of theory and the atomic natural orbital (ANO) basis) also support this observation.[27] As such, the current understanding is that the region of the potential near the cp-HOONO conformer is better thought of as a flat shelf rather than a stabilized conformer, analogous to the shelf in the E $^1\Sigma_g^+$ state of the lithium dimer.[28−30]

* To whom correspondence should be addressed. Tel: (215) 898-4640. Fax: (215) 573-2112. E-mail: milester@sas.upenn.edu (M.I.L.); Tel: (614) 292-9694. Fax: (614) 292−1685. E-mail: mccoy@chemistry.ohio-state.edu (A.B.M.).

10.1021/jp056959w CCC: $33.50 
Published on Web 04/12/2006

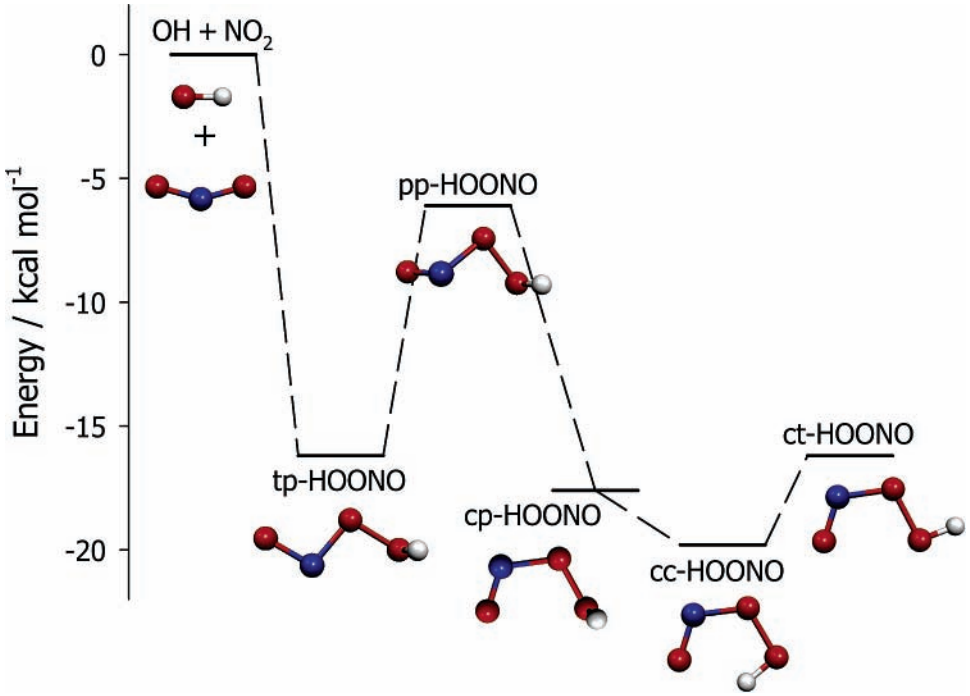


**Figure 1.** Relative energies of stationary points for peroxynitrous acid (HOONO) connected through HOON or OONO torsional motion in relation to the OH + $NO_2$ asymptote. For all depictions of HOONO, the inertial axes are oriented with the *a*-axis horizontal, the *b*-axis vertical, and the *c*-axis perpendicular to the plane. The energies of perp-perp (pp) and trans-perp (tp) configurations are taken from refs 13 and 20, those for cis-perp (cp) and cis-trans (ct) are obtained from ref 16, and that for cis-cis (cc) from refs 4 and 15. The two labels refer to the OONO and HOON torsional angles, respectively.

This paper presents experimental evidence, supported by two-dimensional (2D) theoretical calculations, that HOONO can be observed in cp-like configurations in a pulsed supersonic expansion. A transition originating from a state with predominantly cp character is observed in the first OH overtone region. This spectral feature is attributed to cp-HOONO through a detailed comparison of its transition frequency, rotational constants, transition type, and stability with theoretical predictions.

### Theoretical Predictions of cp-HOONO Properties

To investigate cp-HOONO theoretically, we use the previously reported 2D torsion-stretch potential energy and dipole surfaces of McCoy et al.[16] This potential was based on electronic energies, obtained at the CCSD(T)/cc-pVTZ level of theory/basis, and is described in detail in ref 16. The radial dependence of the potential was based on fits to Morse oscillators, for which the energies were scaled to reproduce the energies along the minimum energy path that were obtained using a cc-pVQZ basis. In contrast, Matthews and Sinha used a similar approach but integrated their slices through the stretch potential numerically.[15] While the models developed in refs 15 and 16 are very similar, there are quantitative differences between them, although, as discussed below, both models are consistent with our interpretation of the present experimental results. Very recently, Schofield et al.[31] reported a 3D surface that incorporates the OOH bend dependence into the 2D model of Matthews and Sinha.[15]

For the present analysis, we employ an adiabatic separation of the fast OH stretch coordinate and the slower HOON torsion, $\tau$. For each value of $\tau$, we take a 1D cut along the OH distance coordinate, $r_{OH}$, and this radial slice is used to evaluate the $\tau$-dependence of the energy in the OH stretch and the associated wave functions. The energies of the states with OH in its ground state, $v_{OH} = 0$, and second excited state, $v_{OH} = 2$, are plotted in Figure 2. The associated wave functions are used to obtain

$$\vec{\mu}_{2,0}(\tau) = \int \psi_{v_{OH}=2}(r_{OH};\tau)\vec{\mu}(r_{OH},\tau)\psi_{v_{OH}=0}(r_{OH};\tau)\, dr_{OH} \qquad (1)$$

The resulting functions are plotted in Figure 3. Using these 1D potential and dipole functions, we evaluate the torsional wave functions and energies and, from them, the associated oscillator strengths. These are reported in Table 1. For comparison, we also give the results reported by Matthews and Sinha.[15]

We find that transitions from the $n'' = 3$ torsional state to the states with $n' = 3$, 4, or 5 have among the largest oscillator strengths of the calculated $2 \leftarrow 0$ transitions of the OH stretch ($\nu_{OH}$) and, as is seen in the results reported in Table 1, these oscillator strengths differ by roughly a factor of 2. If we look at the corresponding probability amplitudes, we find that the $n'' = 3$ state and the $n' = 4$ and 5 states have most of their probability amplitude, $\geq$75%, in the cp-HOONO shelf region of the potential with $60° < |\tau| < 120°$. As such, while the electronic structure calculations provide compelling evidence that the minimum in the HOONO torsion potential is not sufficiently deep to support bound states in the cp-HOONO geometry, there are nevertheless states that appear to be localized predominantly in this region. The existence of such states reflects the dramatic increase in the available configuration space at energies of 2600 and 9500 $cm^{-1}$ for the adiabatic potentials with $v_{OH} = 0$ and 2, respectively. This leads to shelf states with substantially different properties than lower-lying states primarily because they sample different regions of coordinate space. The cp-HOONO terminology utilized hereafter in this paper refers to quantum state(s) with substantial probability amplitude ($\geq$75%) in cis-perp configurations characteristic of this shelf region. Finally, the cp shelf states have different *n* quantum labels for $v_{OH} = 0$ and 2, reflecting the fact that the cc-HOONO well becomes deeper as $v_{OH}$ is increased due to hydrogen

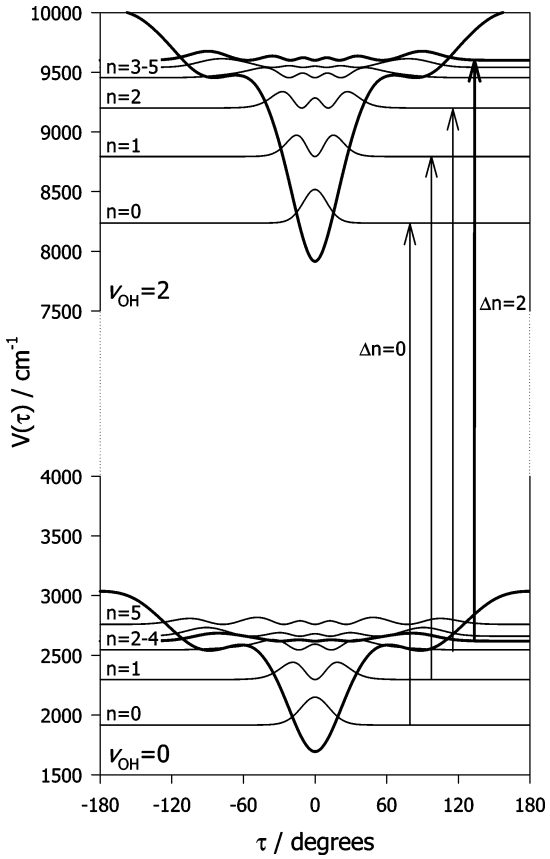


**Figure 2.** Vibrationally adiabatic potentials for the $v_{OH} = 0$ and 2 states of HOONO plotted as a function of the HOON torsional angle $\tau$ that connects the cis-cis (cc) global minimum with cis-perp (cp) configurations. The probability densities and corresponding energies of the six lowest torsional states, $n = 0-5$, associated with each $v_{OH}$ vibrational level are shown, along with arrows indicating OH overtone transitions with $\Delta n = 0$ from cc configurations ($n'' = 0-2$) and $\Delta n = 2$ from a cp configuration ($n'' = 3$).

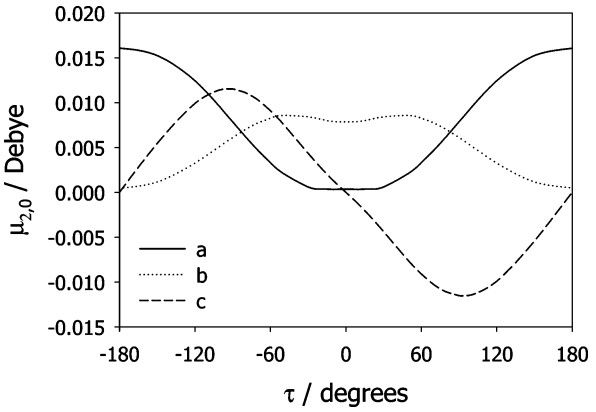


**Figure 3.** Components of the transition dipole moment $\mu_{2,0}$ associated with the $v_{OH} = 0$ to 2 overtone transition of HOONO along the three inertial axes. The relative contributions of the *a*, *b*, and *c* components of the transition dipole moment change significantly with the HOON torsional angle $\tau$.

bonding and the associated decrease in the OH stretch frequency of the cc-HOONO conformer.[16]

In Figure 3, the three components of the transition dipole moment between the states with $v_{OH} = 0$ and 2, $\mu_{2,0}$, are plotted as a function of $\tau$. As shown in the figure, the *a* and *b* components are symmetric with respect to $\tau = 0$, whereas the *c* component is antisymmetric. Since the torsional potential is symmetric with respect to $\tau = 0$, the OH overtone transitions with $\Delta n = 1$ will be *c*-type, while those with $\Delta n = 0$ or 2 will be a combination of *a*- and/or *b*-type.

**TABLE 1: Calculated Properties of OH Overtone Transitions ($v_{n',n''}$) of HOONO Involving Torsional Excitation Based on the 2D Potential Surface in ref 16**

| $n''$ | $n'$ | $v_{n',n''}$ (cm$^{-1}$) | $a$[a] | $b$ | $c$ | relative oscillator strength[b] | oscillator strength ($\times 10^7$) |
|---|---|---|---|---|---|---|---|
| 0 | 0 | 6322 | 0.002 | 0.998 | 0.000 | 1.000 | 1.845 |
| | | 6485[c] | | | | | 2.76[c] |
| 3 | 3 | 6835 | 0.191 | 0.594 | 0.000 | 0.785 | 1.449 |
| | | 6809 | | | | | 2.22 |
| 3 | 4 | 6921 | 0.000 | 0.000 | 1.704 | 1.704 | 3.144 |
| | | 6944 | | | | | 2.30 |
| 3 | 5 | 6981 | 0.578 | 0.215 | 0.000 | 0.793 | 1.463 |
| | | 7024 | | | | | 1.46 |

[a] *a*, *b*, and *c* represent the contribution of $\alpha$th component of the dipole moment to the oscillator strength for the $n' \leftarrow n''$ transition. [b] These numbers are normalized to the oscillator strength of the $0 \leftarrow 0$ transition. [c] Second entries of transition frequency and oscillator strength are taken from Matthews and Sinha (ref 15).

As seen in the results reported in Table 1, the $4 \leftarrow 3$ transition is predicted to be a purely *c*-type transition at 6921 cm$^{-1}$, while the $5 \leftarrow 3$ transition is computed to have an *a:b* ratio of roughly 3:1 and a frequency of 6981 cm$^{-1}$. Using these wave functions, we also evaluate the vibrationally averaged values of the rotational constants for the $n'' = 3$ state. They are 0.7101, 0.2506, and 0.1883 cm$^{-1}$ which are close to the values obtained by diagonalizing the moment of inertial tensor at $\tau = 90°$, 0.7129, 0.2473, and 0.1871 cm$^{-1}$.

## Experimental Methods

The experimental technique for generating HOONO in a pulsed supersonic expansion has been described previously.[19-21] Briefly, the vapor from nitric acid ($HONO_2$, 100% fuming) is entrained in Ar or Ne carrier gas (80 psi) and photolyzed with the 193 nm output of an ArF excimer laser. Photolysis takes place within a quartz capillary tube attached to the exit of a pulsed valve assembly. The photolytically generated OH and $NO_2$ radicals undergo three-body association reactions in the high-pressure environment of the capillary tube, leading to the regeneration of $HONO_2$ as well as the formation of the desired HOONO product. The newly formed HOONO and other species present in the gas mixture are subsequently cooled in the supersonic expansion.

An IR pump−UV probe technique is utilized for detection of HOONO in the first OH overtone region. Tunable IR radiation at 1.4 $\mu$m (10 mJ) is produced with an optical parametric oscillator (OPO, Continuum Mirage 3000) pumped by an injection seeded Nd:YAG laser. The OH ($v = 0$) fragments produced by IR excitation are detected by laser-induced fluorescence (LIF) on the A−X (1,0) transition at 282 nm with a frequency-doubled Nd:YAG pumped dye laser. The IR frequency is calibrated by recording a photoacoustic spectrum of $H_2O$ and etalon trace (FSR = 0.2 cm$^{-1}$) or by using a wavelength meter (Coherent WaveMaster, 0.01 cm$^{-1}$ resolution); the UV frequency is calibrated using the well-known positions of OH lines.[32,33] The IR and UV laser beams are spatially overlapped with minimal time delay (20 ns) at the crossing with the supersonic expansion. The IR pump laser (10 Hz) is present for every other UV probe laser pulse (20 Hz), which permits data acquisition with active background subtraction of any UV only signal.[20,21]

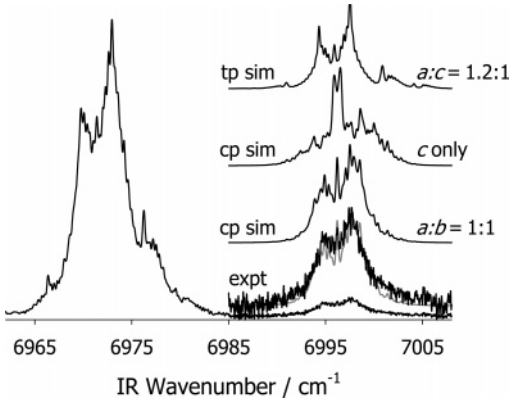


**Figure 4.** Infrared action spectrum of HOONO in the OH overtone region recorded with the UV probe laser fixed on the OH A−X (1,0) $Q_1(9/2)$ transition. The spectrum shows the OH overtone transition of tp-HOONO at 6971.4 $cm^{-1}$ as well as a weaker feature at 6996.2 $cm^{-1}$. An expanded version of the weaker feature is compared with simulations of rotational band contours predicted for cp-HOONO and tp-HOONO under the present experimental conditions. A simulation of cp-HOONO with an *a:b* ∼ 1:1 ratio, homogeneous line width of 0.3 $cm^{-1}$, and rotational temperature of 5 K provides an excellent representation of the observed band structure.

## Experimental Results

The trans-perp (tp) conformer of HOONO has been previously identified by this group in the first and second OH overtone regions under jet-cooled conditions and assigned based on the vibrational frequency, rotational band structure, and transition type of these features.[19−21] The first OH overtone of tp-HOONO has its band origin at 6971.4 $cm^{-1}$ (see Figure 4), while the second overtone is centered at 10195.3 $cm^{-1}$ (origin). Under thermal conditions, most features observed in the first and second OH overtone regions have been assigned to the cis-cis (cc) conformer of HOONO,[12−16] including some with torsional excitation that access cp-like configurations, although the first OH overtone of tp-HOONO has also been observed.[13] By contrast, the cc-HOONO conformer has not been detected in the first overtone region under jet-cooled conditions,[20] because a combination of its lower OH overtone transition frequency, 6365 $cm^{-1}$ (cc), and greater binding energy prevents dissociation, which is required for action spectroscopy measurements. The first OH overtone spectrum of cc-HOONO, obtained under thermal conditions, also exhibits a reduced quantum yield for features below ∼6940 $cm^{-1}$.[13] This suppresses lower-energy features relative to hot bands originating from excited torsional levels that appear at higher frequency.[15,16]

In addition to the OH overtone transition of tp-HOONO, several weaker features were previously reported in the first overtone region under jet-cooled conditions.[20] At the time, however, only the highest energy feature at 7237 $cm^{-1}$ could be definitively assigned as a combination band of tp-HOONO involving two quanta of OH stretch and one quantum of the low-frequency HOON torsion. To enhance the signals associated with the other weaker features, we further optimized the photolytic production of HOONO and reduced the distance (*x*) between the exit of the quartz capillary tube ($D = 0.5$ mm orifice) and the laser crossing to $x/D = 20$ (from $x/D = 30$) to increase the number density in the laser interaction region. These same improvements were utilized to enhance the second OH overtone spectrum of tp-HOONO.[21]

Under these improved conditions, the rotational band contour of the weak feature at 6996.2 $cm^{-1}$ (origin) has emerged, enabling it to be more fully characterized. This feature lies 24.8 $cm^{-1}$ to higher energy of the first OH overtone band of tp-HOONO, as shown in the survey scan of Figure 4, recorded with the UV probe laser fixed on the $Q_1(4)$ line of the OH A−X (1,0) transition which optimized the signal. This feature lies very close to the predicted location for the OH overtone transition of cp-HOONO with $\Delta n = +2$ at 6981 $cm^{-1}$ (or 7024 $cm^{-1}$ in ref 15). It also falls within the dominant feature seen in thermal action spectra at 6935 $cm^{-1}$ that spans ∼200 $cm^{-1}$,[12−14] which has recently been ascribed to overtone transitions originating from torsionally excited states with substantial cp character.[15,16]

An enlarged view of the feature at 6996.2 $cm^{-1}$ along with simulations of rotational band structures predicted for tp- and cp-HOONO are also shown in Figure 4. The upper simulation uses the rotational constants and transition type (*a:c* = 1.2:1) previously established for the first overtone of tp-HOONO and estimates for the homogeneous line width ($\Gamma = 0.3$ $cm^{-1}$) and rotational temperature ($T_{rot} \sim 5$ K).[34] The tp-HOONO simulation fails to reproduce the observed band structure, as evident from the sharp delineation of the two central *c*-type Q-branches in the simulation, which is characteristic of the extended, open structure of the near-prolate asymmetric top ($\kappa = -0.988$).

The experimental rotational band structure of the 6996.2 $cm^{-1}$ feature is much more closely reproduced by a simulation of cp-HOONO using the theoretically predicted rotational constants and one of two possible transition types. The simulations utilize the vibrationally averaged rotational constants predicted for $n'' = 3$ (assumed unchanged upon OH overtone excitation), along with estimates for the transition types of an OH overtone band with $\Delta n = +1$ (*c*-type only) and $\Delta n = 0, +2$ (*a:b* hybrid band). The cp simulations use the same estimates for $\Gamma$ and $T_{rot}$, given above. The *c*-only simulation for the $\Delta n = +1$ transition can be readily excluded because it does not match the observed band structure, in addition to the mismatch with the predicted transition frequency (6921 $cm^{-1}$). A cp simulation with *a:b* ∼ 1:1 reproduces the observed band contour, as shown in Figure 4 as a separate trace and superimposed on the experimental data. The predicted transition frequency makes the $\Delta n = +2$ assignment most likely, as discussed below. This cp simulation has a different appearance than that for tp-HOONO because the cis configuration of the heavy atoms results in considerably different rotational constants, which are further away from the prolate top limit ($\kappa = -0.761$) as shown in Figure 1. This increased asymmetry strongly affects the *b*-type component of the hybrid band, reducing the energy spacing between the central Q-branches and increasing the shading of *K* stacks in all branches, with the net effect of filling in the central region of the band contour.

It should be noted that a cc-HOONO feature would exhibit a similar rotational band contour since the cc rotational constants (0.7140, 0.2651, and 0.1932 $cm^{-1}$), determined experimentally,[17] are similar to those predicted for cp-HOONO, although transitions originating from cc ($n'' = 0$) and cp ($n'' = 3$) configurations are predicted to have different *a:b* ratios (see Table 1). Nevertheless, the pure OH overtone and combination bands of cc-HOONO originating from the ground state of the cc conformer can be excluded based on energetic considerations discussed below.

The quantum state distribution of the OH X $^2\Pi_{3/2}$ ($v = 0$) products resulting from IR excitation provides additional information about the initial state. For these experiments, the IR laser is fixed on the feature at 6996.2 $cm^{-1}$, while the UV laser is tuned to various lines of the OH A−X (1,0) transition to determine the relative population of the OH products in each internal energy state.[21] As shown in Figure 5, the product state

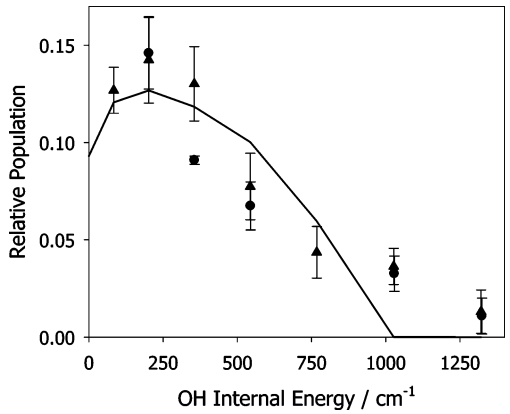


**Figure 5.** Internal energy distribution of the OH X $^2\Pi_{3/2}$ ($v = 0$, $J_{OH}$) fragments observed following excitation of the cp-HOONO feature at 6996.2 $cm^{-1}$. The $\Pi(A'')$ and $\Pi(A')$ $\Lambda$-doublet components are distinguished by circle and triangle symbols, respectively. The curve through the experimental data is predicted from a phase-space theory (PST) statistical calculation.

distribution peaks at $J_{OH} = 7/2$, falls off with increasing OH rotational excitation, and exhibits no $\Lambda$-doublet propensity. The highest energetically open product state is $J_{OH} = 15/2$ with 1029.1 $cm^{-1}$ of internal energy.[35] When this value is combined with the photon energy, we can deduce that the initial state is stabilized by approximately 17.0 kcal $mol^{-1}$, assuming minimal internal excitation of $NO_2$ or translational recoil. This stability is slightly smaller than theoretical predictions for cp-HOONO or an excited torsional state in the cp shelf region,[15,16,22,27] as discussed below. The qualitative form of the OH ($v = 0$) product state distribution is consistent with a statistical dissociation process, as illustrated using phase-space theory (PST) in Figure 5, which was found previously for tp-HOONO.[21] The energy available to the OH + $NO_2$ products in the PST calculation is constrained by the highest open OH product state. A prior distribution[20,21] subject to the same constraint models the data comparably well (not shown).

The stability derived from the product state measurements is much too small for cc-HOONO, which is estimated at 19.8(2) and 19.9(5) kcal $mol^{-1}$ using different experimental methods.[4,15] This eliminates the possibility that the feature at 6996.2 $cm^{-1}$ could be a transition originating from the ground state ($n'' = 0$) of the cc conformer. While such a transition could result in dissociation, it would leave only ~100 $cm^{-1}$ of excess energy for the OH + $NO_2$ fragments. Consequently, only the very lowest rotational states of OH, specifically $J_{OH} = 3/2$ and 5/2, could be populated, in stark contrast to the observed product state distribution (Figure 5).

## Discussion

In summary, the weak feature observed at 6996.2 $cm^{-1}$ using infrared action spectroscopy is attributed to the OH overtone transition of cp-HOONO with $\Delta n = +2$ due to its transition frequency, rotational constants, transition type, and product state distribution. The observed transition frequency is in remarkably good agreement with the theoretically predicted frequency of 6981 $cm^{-1}$ (or 7024 $cm^{-1}$ in ref 15), and the calculated rotational constants provide a very good representation of the experimental rotational band contour. The *a:b* ratio predicted theoretically for the $\Delta n = +2$ transition is somewhat greater than the observed transition type (*a:b* ~ 1:1). Figure 3 shows that the relative contributions of the *a* and *b* components of the transition dipole moment $\mu_{2,0}$ change significantly with the HOON torsional angle $\tau$. The OH overtone transition is predominantly *b*-type at 0° (cc), nearly equal *a*- and *b*-type contributions at 90° (cp), and increasingly *a*-type at larger angles (ct). The experimental *a:b* ratio suggests a slightly smaller average torsional angle, ~90°, or perhaps more localization in cp configurations than predicted theoretically. Finally, the observed OH ($v = 0$) product state distribution yields a stability for cp-HOONO of 17.0 kcal $mol^{-1}$, corresponding to ~0.8 kcal $mol^{-1}$ more stable than tp-HOONO[20] and ~2.6 kcal $mol^{-1}$ less stable than cc-HOONO, with the cc conformer assumed to be 3.4 kcal $mol^{-1}$ more stable than tp-HOONO.[8] Most recent theoretical calculations place cp-HOONO at 1.4 to 2.0 kcal $mol^{-1}$ above cc-HOONO using purely electronic or zero-point corrected energies.[15,16,22,27] The experiment indicates that cp-HOONO is somewhat less stable than predicted theoretically, suggesting the need for a full dimensionality calculation of the cp-HOONO vibrational energy.

We exclude the alternate possibility of a $\Delta n = 0$ transition of cp-HOONO ($n'' = 3$), which is expected to have a similar band contour, because the predicted transition frequency is quite far from the observed position. The $\Delta n = 0$ transition of cp-HOONO ($n'' = 3$) is expected to appear at a much lower frequency, 6835 $cm^{-1}$ based on 2D calculations (or 6809 $cm^{-1}$ in ref 15). In addition, the ($n''$,$n'$) = (3,3) transition of cp-HOONO is roughly estimated at an even lower frequency of 6740 $cm^{-1}$ from an anharmonic fit to prior experimental reports of ($n''$, $n'$) = (0,0), (1,1), and (2,2) transitions at 6365, 6505, and 6630 $cm^{-1}$.[13]

Of course, we have also searched for the $\Delta n = +1$ and 0 transitions of cp-HOONO predicted to occur at 6921 and 6835 $cm^{-1}$ (Table 1). We have observed a 2−3 times weaker feature at 6914.8 $cm^{-1}$ with the sharp central peak anticipated for a $\Delta n = +1$ transition, but the feature is too weak to permit a definitive assignment. No additional features were observed in scans from 6810 to 7360 $cm^{-1}$, aside from those reported previously.[20] Thus, it appears that the $\Delta n = +1$ and 0 transitions of cp-HOONO are weaker than anticipated from the 2D model, suggesting that at least some of the remaining seven vibrational degrees of freedom are important in determining oscillator strengths.

The observation of a cp-HOONO transition demonstrates that torsional states with cp-like configurations (e.g., $n'' = 3$) are populated under pulsed supersonic jet conditions. Population is retained in the torsional states for at least 50 $\mu$s as HOONO moves from the excimer photolysis position to the IR pump/UV probe region while undergoing many collisions with the carrier gas that cool it to a rotational temperature of ~5 K. The observation of a transition originating from cp-HOONO suggests that there may be a dynamical bottleneck that slows relaxation from $n'' = 3$ to lower $n''$ levels. This could arise from the enormous change and reduction in configuration space required to shift from cp-like configurations ($60° < |\tau| < 120°$) to the restricted, albeit more stable, cc-HOONO structure ($|\tau| \leq 15°$) and formation of the intramolecular hydrogen bond.

Finally, we provide an update on two additional weaker features previously reported in this spectra region at 6938 and 6960 $cm^{-1}$,[20] which are currently thought to be the first OH overtone transition of $HONO_2$ and an Ar complex, respectively. The latter feature was absent in Ne carrier gas, although the other weaker features including cp-HOONO remained. The $HONO_2$ feature appears to have been detected by a vibrationally mediated photodissociation scheme,[36] which requires two photons from the UV laser pulse: one promotes vibrationally excited $HONO_2$ to a dissociative electronic state and another detects the OH X $^2\Pi$ ($v = 0$) fragments from the dissociation

event. The $HONO_2$ feature is readily observed by another detection scheme utilizing $NO_2$ chemiluminescence,[36] which clearly reveals a Fermi resonance[37] involving two other states that will be reported elsewhere.[38]

**Acknowledgment.** This research was sponsored by grants to M.I.L. and A.B.M. from the Chemistry Division of the National Science Foundation. The authors thank John F. Stanton for sharing his CCSD(T)/ANO ab initio calculations for HOONO prior to publication.

## References and Notes

(1) Finlayson-Pitts, B. J.; Pitts, J. N. *Chemistry of the Upper and Lower Atmosphere: Theory, Experiments, and Applications*; Academic Press: San Diego, CA, 2000.

(2) Golden, D. M.; Smith, G. P. *J. Phys. Chem. A* **2000**, *104*, 3991.

(3) Donahue, N. M.; Mohrschladt, R.; Dransfield, T. J.; Anderson, J. G.; Dubey, M. K. *J. Phys. Chem. A* **2001**, *105*, 1515.

(4) Hippler, H.; Nasterlack, S.; Striebel, F. *Phys. Chem. Chem. Phys.* **2002**, *4*, 2959.

(5) Golden, D. M.; Barker, J. R.; Lohr, L. L. *J. Phys. Chem. A* **2003**, *107*, 11057.

(6) McGrath, M. P.; Rowland, F. S. *J. Phys. Chem.* **1994**, *98*, 1061.

(7) Dixon, D. A.; Feller, D.; Zhan, C.-G.; Francisco, J. S. *J. Phys. Chem. A* **2002**, *106*, 3191.

(8) Bean, B. D.; Mollner, A. K.; Nizkorodov, S. A.; Nair, G.; Okumura, M.; Sander, S. P.; Peterson, K. A.; Francisco, J. S. *J. Phys. Chem. A* **2003**, *107*, 6974.

(9) Cheng, B. M.; Lee, J. W.; Lee, Y. P. *J. Phys. Chem.* **1991**, *95*, 2814.

(10) Lo, W.-J.; Lee, Y. P. *J. Chem. Phys.* **1994**, *101*, 5494.

(11) Zhang, X.; Nimlos, M. R.; Ellison, G. B.; Varner, M. E.; Stanton, J. F. *J. Chem. Phys.* **2006**, *124*, 084305.

(12) Nizkorodov, S. A.; Wennberg, P. O. *J. Phys. Chem. A* **2002**, *106*, 855.

(13) Fry, J.; Nizkorodov, S. A.; Okumura, M.; Roehl, C. M.; Francisco, J. S.; Wennberg, P. O. *J. Chem. Phys.* **2004**, *121*, 1432.

(14) Matthews, J.; Sinha, A.; Francisco, J. S. *J. Chem. Phys.* **2004**, *120*, 10543.

(15) Matthews, J.; Sinha, A. *J. Chem. Phys.* **2005**, *122*, 104313.

(16) McCoy, A. B.; Fry, J. L.; Francisco, J. S.; Mollner, A. K.; Okumura, M. *J. Chem. Phys.* **2005**, *122*, 104311.

(17) Drouin, B. J.; Fry, J. L.; Miller, C. E. *J. Chem. Phys.* **2004**, *120*, 5501.

(18) Fry, J. L.; Drouin, B. J.; Miller, C. E. *J. Chem. Phys.* **2006**, *124*, 084304.

(19) Pollack, I. B.; Konen, I. M.; Li, E. X. J.; Lester, M. I. *J. Chem. Phys.* **2003**, *119*, 9981.

(20) Konen, I. M.; Pollack, I. B.; Li, E. X. J.; Lester, M. I.; Varner, M. E.; Stanton, J. F. *J. Chem. Phys.* **2005**, *122*, 094320.

(21) Konen, I. M.; Li, E. X. J.; Stephenson, T. A.; Lester, M. I. *J. Chem. Phys.* **2005**, *123*, 204318.

(22) McGrath, M. P.; Rowland, F. S. *J. Chem. Phys.* **2005**, *122*, 134312.

(23) Schofield, D. P.; Kjaergaard, H. G. *J. Phys. Chem. A* **2005**, *109*, 1810.

(24) Zhao, Y.; Houk, K. N.; Olson, L. P. *J. Phys. Chem. A* **2004**, *108*, 5864.

(25) Zhang, J.; Dransfield, T.; Donahue, N. M. *J. Phys. Chem. A* **2004**, *108*, 9082.

(26) Ellison, G. B. Personal communication, 2005.

(27) Varner, M. E.; Stanton, J. F. Personal communication, 2005.

(28) Jastrzebski, W.; Pashov, A.; Kowalczyk, P. *J. Chem. Phys.* **2001**, *114*, 10725.

(29) Papanikolas, J. M.; Williams, R. M.; Leone, S. R. *J. Chem. Phys.* **1997**, *107*, 4172.

(30) Bernheim, R. A.; Gold, L. P.; Tomczyk, C. A.; Vidal, C. R. *J. Chem. Phys.* **1987**, *87*, 861.

(31) Schofield, D. P.; Kjaergaard, H. G.; Matthews, J.; Sinha, A. *J. Chem. Phys.* **2005**, *123*, 134318.

(32) Dieke, G. H.; Crosswhite, H. M. *J. Quant. Spectrosc. Radiat. Transfer* **1962**, *2*, 97.

(33) Luque, J.; Crosley, D. R. *LIFBASE: Database and Spectral Simulation Program*, version 1.5; SRI International Report MP 99-009; 1999.

(34) The HOONO vibrational temperature is not known, although vibrational temperatures are typically somewhat higher than the rotational temperatures in a supersonic jet. It is worth noting that we have not observed other "hot bands" originating from excited torsional states of tp- or cc-HOONO. On this basis, we assume that we do not have a thermal distribution of population in the torsional states of cc-HOONO.

(35) A careful examination of the next higher product state shows it to be closed within our experimental uncertainty, in contrast with a preliminary report that suggested it was open (ref 20).

(36) Sinha, A.; Vander Wal, R. L.; Crim, F. F. *J. Chem. Phys.* **1989**, *91*, 2929.

(37) Feierabend, K. J.; Havey, D. K.; Vaida, V. *Spectrochim. Acta, Part A* **2004**, *60*, 2775.

(38) Konen, I. M.; Li, E. X. J.; Lester, M. I.; Vazquez, J.; Stanton, J. F. Manuscript in preparation, 2005.